# In situ Quality Assessment of a Novel Underwater $pCO_2$ Sensor Based on Membrane Equilibration and NDIR Spectrometry

PEER FIETZEK

*GEOMAR Helmholtz Centre for Ocean Research Kiel, and CONTROS Systems & Solutions GmbH, Kiel, Germany*

BJÖRN FIEDLER, TOBIAS STEINHOFF, AND ARNE KÖRTZINGER

*GEOMAR Helmholtz Centre for Ocean Research Kiel, Kiel, Germany*

(Manuscript received 22 April 2013, in final form 24 July 2013)

ABSTRACT

This paper presents a detailed quality assessment of a novel underwater sensor for the measurement of $CO_2$ partial pressure ($pCO_2$) based on surface water field deployments carried out between 2008 and 2011. The commercially available sensor, which is based on membrane equilibration and nondispersive IR (NDIR) spectrometry is small and can be integrated into mobile platforms. It is calibrated in water against a proven flow-through $pCO_2$ instrument within a custom-built calibration setup. The aspect of highest concern with respect to achievable data quality of the sensor is the compensation for signal drift inevitably connected to absorption measurements. Three means are used to correct for drift effects: (i) a filter correlation or dual-beam setup, (ii) regular zero gas measurements realized automatically within the sensor, and (iii) a zero-based transformation of two sensor calibrations flanking the time of sensor deployment.

Three sensors were tested against an underway $pCO_2$ system during two major research cruises, providing an in situ temperature range from 7.4° to 30.1°C and $pCO_2$ values between 289 and 445 $\mu$atm. The average difference between sensor and reference $pCO_2$ was found to be $-0.6 \pm 3.0$ $\mu$atm with an RMSE of 3.7 $\mu$atm.

## 1. Introduction

The measurement of dissolved carbon dioxide ($CO_2$) in seawater is important and valuable for a large number of scientific, industrial, and socioeconomic issues. Major scientific interest is related to the anthropogenic increase of atmospheric $CO_2$ concentrations and the resulting oceanic uptake of this most important anthropogenic greenhouse gas (Sabine et al. 2004; Rogner et al. 2007). The exchange of $CO_2$ across the air–sea interface and the dynamics and trends of the carbon cycle in coastal and open ocean regions (Takahashi et al. 2009; Gruber et al. 2010) as well as in the interior ocean are key aspects of current marine carbon cycle research.

Dissolved $CO_2$ reacts with water to form carbonic acid ($H_2CO_3$), which rapidly dissociates into hydrogen ($H^+$), bicarbonate ($HCO_3^-$), and carbonate ions ($CO_3^{2-}$). The exact speciation within the marine $CO_2$ system—that is, between the above-mentioned species of the carbonic acid dissociation system—strongly affects the pH of seawater (Millero 2007) and is of major interest. An increasing amount of dissolved $CO_2$ therefore leads to a decreasing pH, a process also referred to as ocean acidification in the context of the anthropogenic $CO_2$ transient. Its impact on calcifying organisms as well as on the physiology and reproduction of other marine species is presently not well understood (Doney et al. 2009). The potential long-term influence of acidification on fisheries but also carbon capture and underwater storage scenarios (Metz et al. 2005) show the socioeconomic relevance of $CO_2$ measurements and highlight the demand for baseline monitoring of $CO_2$ parameters in the ocean.

Since the thermodynamic constants of the marine carbonate systems are known rather precisely (e.g., Millero 2007), the marine $CO_2$ system can be fully determined by measurement of any two of the following variables: dissolved inorganic carbon (DIC), total alkalinity (TA), pH and $CO_2$ fugacity ($fCO_2$), or $CO_2$ partial pressure ($pCO_2$; Millero 2007). Although the sole

*Corresponding author address:* Peer Fietzek, GEOMAR Helmholtz Centre for Ocean Research Kiel, Düsternbrooker Weg 20, 24105 Kiel, Germany.
E-mail: pfietzek@geomar.de

DOI: 10.1175/JTECH-D-13-00083.1

measurement of $pCO_2$ is not sufficient to fully characterize the marine $CO_2$ system, $pCO_2$ is still a useful parameter on its own: It is the determining factor for air–sea gas exchange and responds sensitively to biogeochemical processes such as photosynthesis and respiration. Hence, $pCO_2$ is both, a valuable stand-alone measurement parameter and a useful measured variable within multiparameter measurements for the determination of the $CO_2$ system. So far only $pCO_2$ and pH can be measured autonomously with commercial underwater sensors (DeGrandpre et al. 1995; Seidel et al. 2008; Martz et al. 2010). Sensors for autonomous measurements of the other carbonate system parameters TA and DIC (Byrne et al. 2002; Wang et al. 2007) and even for direct measurements of carbonate ions are under development (Byrne and Yao 2008).

Because of a lack of a commercially available underwater $pCO_2$ sensor with a sufficient accuracy and platform integratability expressed by adequate dimensions, an appropriately short response time at surface and at depth, as well as by the ability for continuous measurements, we have advanced the development of an autonomous and commercially produced underwater $pCO_2$ sensor (HydroC-$CO_2$, CONTROS GmbH, Kiel, Germany). Its versatility and specifications allow for integration into various platforms and provide a suitable tool for $pCO_2$ measurements at an improved spatial and temporal resolution in the water column. Here, we present a comprehensive overview of the sensor's measurement principle, its key components, and its calibration. We also assess the achievable data quality by means of a detailed analysis of data from surface water field applications. Measurements against a proven flow-through system only represent one application of the sensor, but at the same time enable the clearest assessment of the sensor's data quality. Many further applications in the water column are possible that best require dedicated discussions such as the measurements on a profiling float presented in Fiedler et al. (2013).

### a. Suitable sensor platforms

Beside classical mobile sensor platforms on the one hand, such as voluntary observing ships (VOS) or research vessels (R/Vs), and stationary buoys and moorings on the other hand, innovative mobile platforms are receiving growing interest (Fietzek et al. 2011). These platforms—for example, autonomous underwater vehicles (AUV), profiling floats, and gliders—provide an increased autonomy, mobility, and versatility as opposed to the classical carriers. They allow for a more cost-efficient data collection on so far largely unexplored temporal and spatial scales. These newly accessible scales are of high interest for the investigation of various biogeochemical processes, making these modern mobile platforms desirable carriers for $pCO_2$ sensors (Gruber et al. 2010). By equipping autonomous platforms as a regional or global sensor array with high spatiotemporal resolution, such as the prominent Argo project, a high scientific potential can be achieved (Roemmich et al. 2009; Johnson et al. 2009; Fiedler et al. 2013). However, in order to be easily installed on modern mobile platforms, new sensors need to cope with the demands of the more complex carriers and fulfill the more stringent requirements with respect to payload capacity, power availability, response time, etc. A more detailed discussion of these facts and circumstances can be found in Fietzek et al. (2011).

### b. $pCO_2$ measurements

The first measurements of dissolved $CO_2$ were developed for medical applications in the 1950s. These were based on wet-chemical pH determination behind a Teflon membrane (Stow et al. 1957; Severinghaus and Bradley 1958). Today, optical $CO_2$ measuring techniques are prevailing. One method is to detect and quantify $CO_2$ molecules within an equilibrated gas stream by means of direct absorption in the infrared (IR) region of the electromagnetic spectrum. Another technique is an indirect measurement making use of the pH-affecting property of $CO_2$ by applying spectrophotometry within an equilibrated pH-sensitive dye solution of known characteristics (DeGrandpre et al. 1995; Lefèvre et al. 1993). An overview of current sensor techniques for carbonate system species can be found in Byrne et al. (2010). A technical evaluation of $pCO_2$ sensors that also includes two sensors of the type discussed here is presented in Tamburri et al. (2011). Between the evaluation and the measurements discussed herein, the status of the sensors was mainly improved through an optimized calibration process and data processing.

The usage of underway flow-through instruments to measure $pCO_2$ both in the oceanic surface layer and in the atmosphere dates back to the 1960s (Takahashi 1961). While in the beginning the application of these systems was restricted to research vessels, current, improved systems are suitable also for application on unattended platforms such as VOS (Watson et al. 2009; Pierrot et al. 2009; Pfeil et al. 2013). Continuous optimization of the overall setup and the components used lead to some standardized design that is nowadays also commercially available. The key components of such a flow-through instrument are the air–seawater equilibrator and the IR gas analyzer. The equilibrator is used to achieve partial pressure equilibrium between the dissolved gases in a continuous stream of seawater and

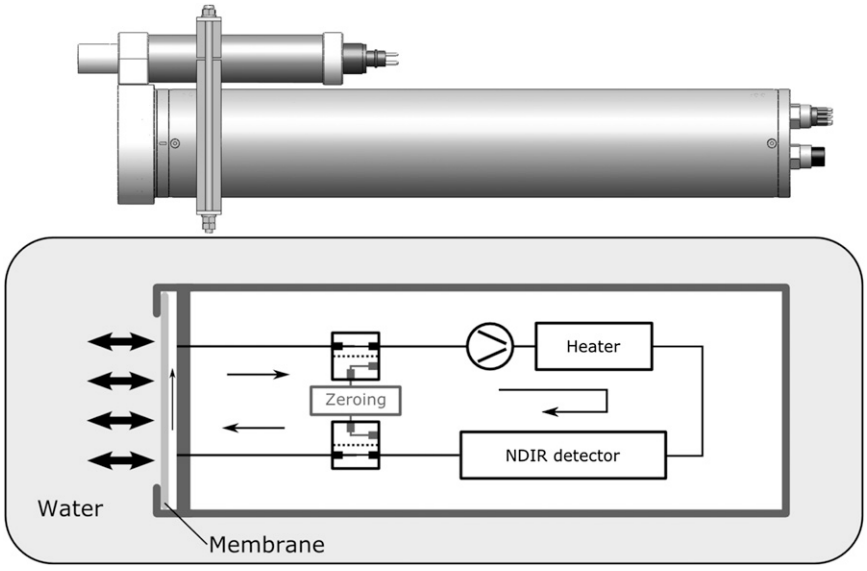


FIG. 1. (top) Drawing of the $pCO_2$ sensor as used in the present study. The sensor is equipped with a water pump (SBE 5T) and a flow head. (bottom) Schematic drawing of the sensor. Partial pressure equilibration occurs at the planar, semipermeable membrane separating the water from the internal head space of approximately 20 mL. A pump continuously circulates the gas between the membrane equilibrator, a heater, and the NDIR detector. Valves can be toggled to realize a zero gas measurement by guiding the gas stream through a soda lime cartridge instead of through the membrane equilibrator.

air that is recirculated between the equilibrator and a benchtop IR analyzer. The achievable measuring accuracy is 2 $\mu$atm for surface seawater $pCO_2$ measurements (Pierrot et al. 2009). The flow-through system data are commonly reported as $pCO_2$, although the $fCO_2$ is the value suggested for most accurate carbonate system calculations. Based on approximated expressions the $fCO_2$, which considers the slightly nonideal behavior of $CO_2$ in the gas phase, can be calculated from temperature and $pCO_2$, which presumes ideal gas behavior.

## 2. Sensor principle and description

### *a. Development and design*

The development aims of the $pCO_2$ sensor among others were to obtain (i) a versatile and autonomous sensor that could be deployed on a profiling float with (ii) a response time of less than five minutes, (iii) an accuracy better than 5 $\mu$atm, and (iv) a stability and reliability that would allow for long-term deployments of several months.

Since the developed sensor is based on the same measuring principle as proven flow-through systems, it has the same key components: an equilibrator and an IR $CO_2$ detector. A planar, semipermeable membrane with a silicone active layer is installed in the head of the sensor. It acts as an equilibrator as well as a phase separator between the ambient water and an internal headspace. The sensor is commonly equipped with a water pump that provides a continuous seawater flow to the membrane and thus reduces the thickness of the static boundary layer in front of the membrane. By that, the response time is effectively shortened and made independent of a relative movement between the membrane and the surrounding water. To withstand high hydrostatic pressures, the membrane is mechanically supported from behind with a sintered metal disc. A gas pump continuously circulates air between the membrane equilibrator and a nondispersive IR (NDIR) detector. Figure 1 shows a model of the sensor and provides a schematic overview of its setup. The gas tightness of the internal gas stream as well as of the integrated valves is checked thoroughly prior to calibration. Opposed to $pCO_2$ underway systems in which gas stream leakages are a major source for measuring errors (Pierrot et al. 2009), the biggest ''leak'' within the gas stream of this sensor remains the equilibration membrane; the high gas permeability of the membrane related to the volume of the gas stream compensates for possible influences caused by small leaks. If bigger leakage occurs within the gas stream, then the entire, much larger internal gas volume of the sensor will be equilibrated, leading to noticeably slower response times but not necessarily biases. The gas

circuit also features a specially developed gas heater upstream of the NDIR detector, whose heating control system is also used to stabilize the temperature of the IR detector. The gas heater buffers seawater temperature gradients ($\Delta T_{\text{in situ}}$) in such a way that large $\Delta T_{\text{in situ}}$ are damped to a much smaller gas temperature gradient. We choose to set the control temperature just high enough for the heating control circuit to keep the controlled temperature stable even at the maximum in situ temperature expected during deployment. When the control temperature is set higher than necessary, avoidably high power consumption is the consequence and the abundant absolute temperature differences between the surrounding water and the internal gas becomes larger. In addition to the gas heater and the temperature stabilization, the sensor's pressure housing is thermally insulated and temperature-sensitive components are separately protected.

Within the gas stream sensors for pressure, temperature, and relative humidity (RH) are installed to determine the conditions within the NDIR detector as well as behind the membrane. Their exact position was chosen upon laboratory tests to be most beneficial for their consideration within the IR sensor data analysis. The quality and a deep understanding of the NDIR detector are crucial for the data quality of both underway instruments and the new underwater sensor. All additional components within the underway instrument's and the underwater sensor's gas circuits beside the equilibrator and NDIR detector, such as the additional sensors mentioned above, are required for accurate and precise absorption measurements and allow for preferably long deployments.

In contrast to the common practice of underway instruments, the absorption measurement within the sensor is carried out in wet air and without interrupting the gas flow for measurement. In the underwater sensor, regular zero gas measurements can be carried out. Therefore, the valves included in the circuit lead the pumped air through a soda lime cartridge instead of the membrane equilibrator at desired intervals (see Fig. 1). In the presence of water vapor, soda lime scrubs the $CO_2$ binding it as calcium carbonate ($CaCO_3$), thus creating a zero gas with respect to $CO_2$.

The sensor operates by consecutively switching through different intervals, the durations of which can be individually set. As soon as the sensor is powered, it starts with a warm-up interval followed by continuous repetition of measuring cycles. One measuring cycle consists of three intervals: zero, flush and measure. The warm-up interval is only passed through once after the sensor has been turned on. The required warm-up time depends on the water temperature and the supplied voltage (cf. Table 1). During the warm-up, the water pump is disabled and data are neither transmitted nor stored in the internal logger. During zero intervals, a zero $CO_2$ gas is created as described above and the sensor provides the current zero reading used later for drift correction. The zeroing typically lasts a few minutes and repetition is recommended at least every 12 h. Data stored during that time are flagged for easy handling during analysis. Flush intervals are only used to flag data acquired during the signal recovery from the zero value to the ambient $pCO_2$ reading. Technically, the measuring process of the sensor does not differ between the flush and the subsequent measuring interval. The time the sensor needs for full equilibration depends on the sensor configuration and the environmental conditions, mainly the water temperature: the warmer the water, the faster the response time and thus the shorter the required flush time. Laboratory and field tests for the response time determination of the sensor as configured

TABLE 1. Specifications of the developed $pCO_2$ sensor as used during the deployments discussed in this paper. The specifications of the currently available sensor model differ from these values with respect to size and power consumption. The power required for the temperature stabilization as well as the warm-up duration depend on the actual water temperature, the chosen control temperature as well as on the thickness of the insulation material. The given warm-up times correspond to a 24-V supply voltage in 20°C water and to 12-V supply voltage in 3°C water. Please refer to the text for further details regarding the warm-up and the zeroing interval. The response times refer to the usage of two different pump models at 20°C water temperature. The pump SBE 5T has a flow rate of approx. 105 mL $s^{-1}$, while the smaller model, SBE 5M, provides a flow rate of approx. 35 mL $s^{-1}$.

| Property | Description/Specification |
|---|---|
| Detector | Single-beam dual-wavelength NDIR detector; zeroings at desired intervals |
| Housing, dimensions | Cylindrical titanium housing, 90 mm × 530 mm (without connector) |
| Depth capability | 2000 m (standard) |
| Weight | 5.5 kg in air, approx 2.6 kg in water |
| Operating temperature | 3°–30°C |
| Supply voltage | 11–24 Vdc |
| Power requirements | <3 W for the detector and all the electronics<br>+<1–3.5 W for temperature stabilization<br>+<6 W during warm-up for 2–30 min<br>+4 W during zeroing<br>+water pump: 7 and 1.5 W (pump SBE 5T and 5M, respectively) |
| Sampling rate | ≤1 Hz |
| Response time ($t_{63\%}$) | Approx 70 and 130 s (pump SBE 5T and 5M, respectively) |
| Measurement range | 200–1000 $\mu$atm (standard) |

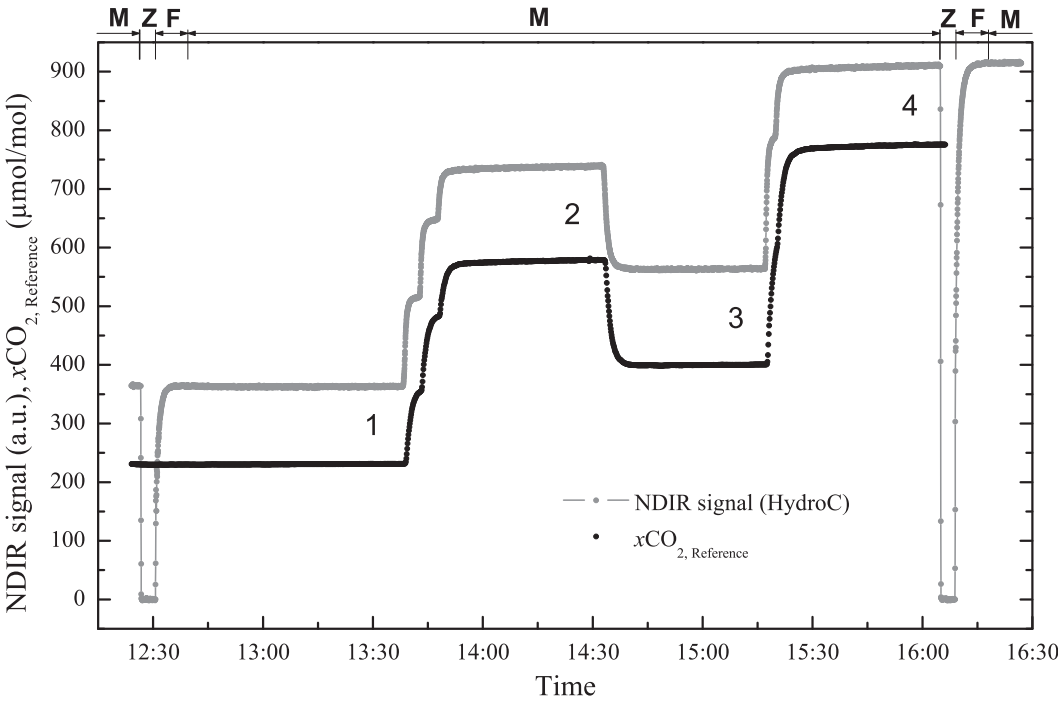


FIG. 2. Course of a calibration carried out at a constant water temperature within the calibration setup described in the text. The absorbance NDIR signal shown in arbitrary units is dual beam and zero corrected. Also shown is the $CO_2$ mole fraction ($xCO_2$) measured by the reference flow-through system. The numbers 1–4 indicate the calibrations steps, and the Z, F, and M mark the sensor intervals: zero, flush, and measure, respectively.

within the deployments presented here indicate a linear dependency of response time on water temperature at a slope of the order of $-1$ s $(1°C)^{-1}$ (data not shown here). Sensor response to a step input can be well described by first-order kinetics and a corresponding exponential fit. Any response time given here hence represents a time constant or a $t_{63\%}$ depending on which formulation is favored. Isothermal pressure vessel experiments up to 200 bar have neither shown indications for a pressure hysteresis, nor could a significant pressure influence on the response time be identified (data not shown here). The actual response time of the sensor can be derived based on the course of the signal recovery during the flush interval as applied by Fiedler et al. (2013). It is typically faster than the 2-min response time of the flow-through system (Pierrot et al. 2009) and allows for measurements on moving platforms, especially when a response time correction is applied to derive the ''true'' ambient $pCO_2$ from the time-lagged sensor signal (Fiedler et al. 2013). A more detailed analysis of the sensor's response characteristics is in preparation. During flush and measurement intervals, the water pump is active and data are recorded as configured. The interval settings simplify the data processing and provide the means to generate measurement data from a fully equilibrated and internally temperature stabilized sensor. Figure 2 shows the sensor signal during calibration with the zero, flush, and measurement intervals indicated.

The comparatively fast response time, small size, and operability of the sensor allow for deployments on various platforms. Because of its design and compared to classical flow-through systems, the maintenance intensity and the risk for leaks in the gas stream are low. If used in situ, the sensor lacks the demand for an accurate water temperature probe, as it is crucial for typical flow-through systems (Körtzinger et al. 2000). To derive the actual amount of dissolved $CO_2$ from the measured partial pressure, the sensor is commonly deployed together with a CTD probe, as the solubility of $CO_2$ depends on temperature and salinity (Weiss 1974).

### *b. Specifications*

Table 1 lists the specifications of the developed sensor as applicable for the measurements discussed in this work. Different data communication options are feasible. An internal datalogger is optional, which can either be used as a stand-alone memory (e.g., Saderne et al. 2013) or for backup storage (e.g., Fiedler et al. 2013). A sleep mode function further facilitates autonomous

installations. The sensor development also comprised a surface water flow-through version of the sensor that is not further addressed here.

### c. $CO_2$ measurements by means of NDIR spectrometry

The properties of the NDIR detector are relevant for the overall performance of the sensor. Drift, cross sensitivities, and the signal-to-noise ratio (S/N) of the NDIR detector directly affect the data quality.

NDIR spectrometry in general is a proven direct measuring technique for mole fractions of gases absorbing in the IR. It is nondestructive and traceable to standards. NDIR detectors for $CO_2$ have small dimensions (several centimeters) and moderate power consumption (here: about 0.5 W) that allow for easy integration. In addition they provide good mechanical strength and are unaffected by vibrations if realized without moving parts. Because of their high selectivity and limited cross sensitivity, NDIR detectors are well suited for qualitative analysis. NDIR detectors are composed of three main components: light source, absorption/beam path, and detector. Each of them has different influences on the final sensor signal and depends differently on environmental variables, for example, temperature. This may lead to complex overall sensor properties. Their choice defines the S/N, the sensitivity, and the measurement range (detection limit and upper range value) of an NDIR unit. The basic idea is to get enough light energy at the desired wavelength to the detector and to make the absorption path sufficiently long such that changes in absorbed light intensity can be clearly resolved by the detector and amplifying electronics. Various options exist to optimize and dovetail these components.

The linear relation between the transmitted light intensity $I$ and molecule concentration $c$ as described by the Beer–Lambert Law makes the technique suitable for quantitative analysis:

$$I = I_0 10^{-\varepsilon c l}, \tag{1}$$

with $I_0$ being the initial light intensity, $l$ is the distance the light travels through the absorbing medium, and $\varepsilon$ is the molar absorption or extinction coefficient of the target molecule to be detected. According to (1) the extinction or absorbance $A$ is defined to be directly proportional to the molecule concentration in the medium:

$$A = \log\left(\frac{I_0}{I}\right) = \varepsilon c l. \tag{2}$$

In reality there is a small nonlinearity between the absorbance measured by the NDIR detector and molecule concentration because the Beer–Lambert law is only defined for a single wavelength of infinitesimal small width, while in applications spectral dependencies occur (Wiegleb et al. 2001).

The NDIR unit used features a blackbody radiator as a broadband IR light source and a pyroelectrical IR detector that requires pulsed operation of the IR emitter. Interference filters in front of the detectors select the desired measurement and reference wavelength and together with electronics for control and evaluation complete the single-beam dual-wavelength NDIR detector. $CO_2$ is typically sensed around 4.26 $\mu$m, where it shows its highest absorption because of its fundamental asymmetric stretching vibration (2349.1 $cm^{-1}$) and the reference wavelength is chosen to be placed in the water vapor window at around 4.0 $\mu$m.

Within an NDIR detector, several temperature influences exist that either require a compensation, calibration, or stabilization. The spectral properties of the filters are temperature dependent: the central filter wavelength can shift and the transmission width can vary. A temperature influence on the sensor can occur in the form of thermal noise, a thermal background signal, and changes in sensitivity. In the case of a dual-beam setup, the influences might even be different for both channels. The emission properties and emitted intensities of the light source show a temperature influence as well. Thermal expansion of the cuvette or other mechanical deformations of the absorption path may have an additional effect on the measurements. Finally, temperature dependencies of the analog electrical components directly behind the detector need to be considered. The overall effect caused by temperature changes is hence both variable in magnitude and sign for measurement channels of two similar products as well as for a measurement and reference channel within the same instrument with separate filters, detectors, and electronics. For this reason and in order to enhance the measurement quality, the entire NDIR detector is temperature stabilized within the sensor. An active temperature stabilization furthermore helps to reduce the required warm-up time present in any NDIR detector because of self-heating effects. A separation of the light source and the detector from the gas stream by windows enhances the temperature stabilization capability and protects the sensitive detector with the filter. A gas heater further reduces the temperature gradient within the cuvette and simultaneously reduces the risk of condensation within the optical components of the sensor.

Any sensor based on an absorption principle such as an NDIR detector senses the highest raw signal in the case of a complete absence of the target molecules in the

beam path, as in that case no absorption occurs and the maximum radiation intensity reaches the detector [see (1)]. Therefore, the regular determination of the sensor signal of a zero gas, the *zeroing*, is essential to account for drift effects that alter the light intensity with time and that otherwise would be erroneously interpreted as changes in target gas concentration. Typical effects are as follows:

1) Intensity variations or spectral shifts of the light source over time
2) Contamination of any component within the beam path that might cause shadowing or growing reflectivity losses in the cuvette
3) Aging effects that alter the detector sensitivity over time
4) Changes in the preamplifier gain of the detector

Within the sensor the zeroing does not only account for long-term drift influences but also for changes of the measurement conditions such as large changes in water temperature that cause internal temperature gradients and different water vapor concentrations within the gas stream.

Drift compensation by means of a differential setup—in our case, realized in the form of filter correlation—is referred to as a two-beam/two-wavelength method. It is supposed to compensate any unwanted influences that cause signal drift of both channels in the same manner (aspects 1 and 2 above) as the measured signal is continuously referenced. Any effects that cause changes in the detector signals and that are not caused by actual concentration changes within the cuvette shall be compensated in real time and parallel to measurements. In reality, this technique has its limitations in accounting for influences resulting from the usage of the two different channels with their own filters and detectors. Theoretically, the zero point of a two-beam instrument should not be affected by the above-mentioned drift reasons (1–4). But as we measure at two different wavelengths, spectral differences and effects related to the two physically different detectors still affect the zero signal of the ''two-beam corrected'' signal. Therefore, we combine the zeroing and the two-beam drift correction means within our sensor. The latter provides a continuous correction applied parallel to measurements, while the zeroing discontinuously further enhances the drift correction capabilities by correcting for effects that differently affect the measured intensities at both detectors. Related to the origin of NDIR detector drift in combination with the dual wavelength setup, it should be pointed out that changes in the zero concentration measurements can (i) occur erratically, especially after transportation of storage, (ii) are not necessarily linear in time with (iii) the slope commonly decreasing over running time or (iv) even changing its sign.

The zero correction of a two-beam sensor signal does not cover concentration-dependent effects that equate to changes in the characteristics of the NDIR sensor's calibration polynomial. Hence, for achieving best accuracies particularly with two-beam NDIR sensors, the sensor in addition to regular zeroings needs to be recalibrated after deployment at different concentrations.

### *d. Membrane equilibration*

The solution-diffusion model can be used to describe gas transport through a dense, semipermeable membrane. Assuming a partial pressure gradient between the water phase and the internal gas stream, the first step within the transport process is adsorption of the molecule at the membrane surface. In the case of a sufficiently small gas concentration, the dissolution process into the membrane can be explained by the Henry–Dalton law, which states the linearity between the partial pressure of a gas and the concentration of that gas in solution connected by a temperature, pressure, and, in the case of seawater, salinity-dependent constant. The dissolution process is followed by diffusion-based transport of the molecules within the membrane along the concentration gradient. Outgassing into the headspace again follows the Henry–Dalton law. This process continues within the membrane of the sensor until partial pressure equilibrium with respect to every single gas component is achieved. Hence, semipermeable membranes can be used as equilibrators for dissolved gas measurements (McNeil et al. 2006). They enable the application of gas-phase-based measuring techniques in an aquatic medium. The time limiting and overall response time dominating step within the entire transport process is the diffusion within the membrane material as well as within a boundary layer in front of the membrane. The permeability of a material is a parameter integrating both the solubility of a gas within the membrane substance and its diffusion constant within the membrane according to Fick's law. Like the solubility and the diffusion coefficient, the permeability is also temperature and pressure dependent as well as concentration independent. The permeabilities of different gases for a given membrane material differ (Robb 1968; Merkel et al. 2000) and hence determine the time constant for the corresponding partial pressure equilibration. The direction of the transport process is defined by the orientation of the individual partial pressure gradient. Silicone, polydimethylsiloxane (PDMS), was chosen as the membrane material because of its high permeability for $CO_2$ (Merkel et al. 2000).

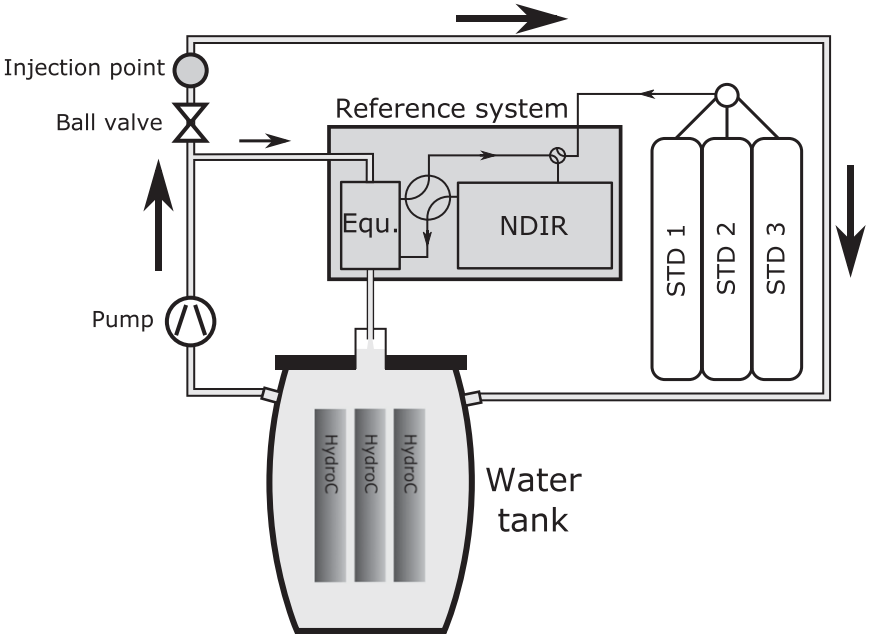


FIG. 3. In-water $pCO_2$ sensor calibration setup. One water pump is used to allow for sufficient mixing of the water in the tank and dispersion of the injected acid and base, as well as to provide water to the reference flow-through system, which is installed in a bypass and whose NDIR unit is regularly calibrated with reference gases.

In addition to all the dissolved gases, water vapor also permeates through the membrane. Its amount within the gas stream is related to the temperature- and salinity-driven water vapor pressure. The risk of condensation within the headspace and especially within the NDIR absorption path induced by steep gradients of warm-to-cold water is minimized by the heating of the gas on its way to the NDIR detector. Furthermore, the permeability of water vapor is more than a magnitude higher than for $CO_2$ (Robb 1968), leading to time constants for water vapor equilibration of about 10 s at the given $CO_2$ response time of about 70 s for this sensor.

Typically, silicone layer thicknesses of around 10 $\mu$m are used. The thickness is determined during membrane production by permeability measurements. Pure silicone monolayer membranes of this thickness could not be easily handled. Therefore, we use thin film composite membranes consisting of the dense silicone layer on top of supporting substructures. In the case of no or minor fouling, the membranes can be deployed for several months to years. Cleaning of the membranes with, for example, diluted sulfuric or oxalic acid at pH 2 has successfully been tested. To avoid physical damage of the thin silicone layer, mechanical cleaning of the membrane surface should be avoided. Instead, the membrane should and can be changed even in the field. The response time of the sensor determined from the flush interval data can also be used to identify organic ongrowth, since heavy fouling slows down the membrane permeation process or the volume rate of pumped water, both of which lead to a reduced response time of the sensor.

## 3. In-water calibration setup

Along with the sensor development, we established a laboratory calibration setup for direct underwater $pCO_2$ calibration (Fig. 3) that can hold up to three sensors simultaneously. An early version of the setup was successfully used in Friedrichs et al. (2010). The setup includes a 120-L insulated and temperature-stabilized water tank. The water temperature can be controlled over the temperature range of 0°–30°C to within ±0.02°C. It is filled with deionized water. Sodium carbonate and bicarbonate are added in the required quantities in order to mimic the $CO_2$ buffer system of seawater (DIC:TA ratio) and thereby allow for a better $pCO_2$ level control. Silver nitrate is added as an antifoulant. Water is continuously pumped through a reference flow-through $pCO_2$ system (Körtzinger et al. 1996) that was slightly modified to suit the laboratory conditions. Additionally, it was equipped with drying components to facilitate continuous reference measurements in dry gas. Special care was taken that the return flow of the

water from the combined bubble-type–laminar-flow equilibrator into the main tank occurs without flow restrictions and thus without altering the pressure conditions within the equilibrator. Temperature probes within the equilibrator and the main tank are regularly calibrated against a reference probe with an accuracy of ±0.02°C. The flow-through system is equipped with a benchtop IR analyzer (LI-6262 or LI-7000, LI-COR, Inc., Lincoln, Nebraska), which is calibrated against three primary [certified National Oceanic and Atmospheric Administration (NOAA) standards] or secondary (referenced to NOAA standards) $CO_2$-in-natural-air standards in the beginning and in the end of each calibration run. Processing of the flow-through system data is carried out according to the procedures described in Dickson et al. (2007) and Pierrot et al. (2009), leading to $pCO_2$ reference values referred to the water temperature in the tank with an accuracy of 2–3 $\mu$atm. During a full calibration run, the $pCO_2$ of the tank water is altered by pH variation through injection of NaOH or HCl solutions. A new concentration in the tank water is set and resolved by the reference system with a time constant of approximately 150 s. By application of the pH-varying technique, a wide $pCO_2$ range can be realized and calibration steps can be set as desired. Since the overall setup cannot be entirely encapsulated from the surrounding air, a small drift of the partial pressures in the tank of typically around 3 $\mu$atm $h^{-1}$ can be observed. Magnitude and time scale of this drift as well as the fact that both the flow-through system and the underwater sensor detect this $pCO_2$ change make this effect negligible with respect to the assumed accuracy of the calibration process. The adjustable range is limited by the measurement range of the IR analyzer of the flow-through system, which is 3000 $\mu$mol $mol^{-1}$ for the dry $CO_2$ mole fraction in the equilibrated gas stream ($xCO_2$). It was found that four calibration steps are sufficient for a sensor calibration in the range of 200–1000 $\mu$atm. The course of a calibration is depicted in Fig. 2.

There are several reasons to calibrate the sensor in water against a proven underway system as opposed to a mere dry gas calibration of the IR detector. The fact that some of the following influences are already considered in data processing corrections or their minimization was addressed in sensor design does not debilitate the following compensatory advantages of an in-water calibration. First, the temperature stabilization, including the gas heater used in the sensor, does not completely avert the presence of temperature gradients within the instrument's housing, components, and gas stream. Hence, the temperature stabilization can only minimize the above-mentioned possible temperature effects on NDIR sensors. An in-water calibration at a temperature as close as possible to the expected temperature in the field helps to further reduce these signal influences. Second, an in-water calibration as described compensates for all effects related to the large absolute humidity present in the sensor's gas stream. These effects are gas–gas interactions, causing band broadening, potential cross sensitivities of the NDIR signal against $H_2O$ because of minor $H_2O$ absorption at the transmitted wavelengths, or $H_2O$ molecule interaction with the cuvette's surface. For a sensor calibration at only one temperature, it is deliberately accepted that the humidity-related compensations are only entirely compensated for a deployment at a water temperature equal to the calibration temperature. Third, an in-water calibration compares the fully processed signal of the instrument with a reference value. Hence, it characterizes the overall instrument, including the entire membrane equilibration process of the headspace as identified, to be important by Byrne et al. (2010). Any not otherwise considered effects occurring in the sensor's gas stream and behind the membrane are taken care of by an in-water calibration.

## 4. Data processing

The dual-beam NDIR detector provides two signals. The raw signal $S_{raw}$ corresponds to the transmitted light intensity around the wavelength at which $CO_2$ efficiently absorbs (4.26 $\mu$m) and the reference signal, $S_{ref}$, expresses the intensity at around 4 $\mu$m, where practically no relevant absorption occurs. Water vapor is a weak absorber at both wavelengths. A continuously referenced sensor signal, the ''two-beam signal,'' is

$$S_{2beam} = \frac{S_{raw}}{S_{ref}}. \quad (3)$$

As a result of the regular zeroing ($Z$), we obtain ''two-beam zero signals'' at discrete points in time:

$$S_{2beam,Z} = \frac{S_{raw,Z}}{S_{ref,Z}}. \quad (4)$$

Linear interpolation in time between two adjacent $S_{2beam,Z}$ provides zero reference signals for every point in time: $S_{2beam,Z}(t)$.

An NDIR signal that is improved by both drift correction (DC) means, dual beam and zeroing, is derived as follows:

$$S_{DC}(t) = \frac{S_{2beam}(t)}{S_{2beam,Z}(t)}. \quad (5)$$

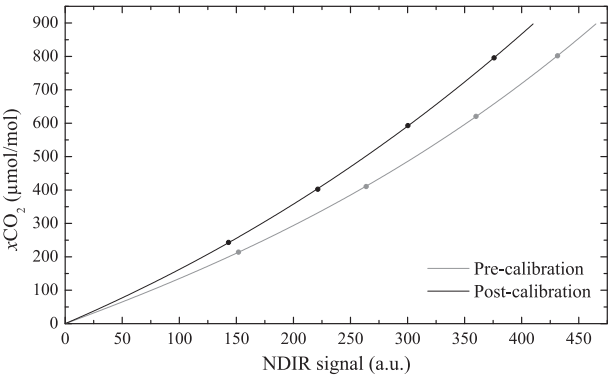


FIG. 4. Calibration polynomials of sensor HC1 before and after the deployment on R/V *Polarstern*. The absorbance NDIR signal is calibrated against the $xCO_2$ within the sensor's gas stream obtained according to the text. The polynomials match the sensor's response characteristics well ($R^2$ in both cases >0.999). A concentration-dependent change in the sensor characteristics between the different points in time (i.e., before and after deployment) of the calibrations is clearly visible in this example for a strongly drifting NDIR sensor.

The final, drift-corrected NDIR signal, which is assumed to be directly proportional to the amount of target molecules in the beam path, is related to $S_{DC}(t)$.

During calibration the flow-through system provides a reference $pCO_2$ for every calibration step. The $pCO_2$ equilibrium is assumed to be established in the membrane equilibrator of the sensor at that time. Using data of the peripheral sensors in the gas stream, the $xCO_2$ in moist air present at the NDIR detector is derived. As the NDIR signal is proportional to the number of molecules in the beam path and not to $xCO_2$, the reference $xCO_2$ needs to be density corrected by using data of the additional temperature and pressure sensors built into the gas stream of the $pCO_2$ sensor. A polynomial of rank 3 with a forced zero crossing is then used to calibrate the individual sensor characteristics. It correlates the absorbance signal of the NDIR detector with the corresponding and density-corrected $xCO_2$ in the gas stream (cf. Fig. 4). Now, all required dependencies are known and the sensor provides the $pCO_2$ based on the absorbance signal of its NDIR detector in combination with the data of the peripheral sensors in its gas stream. Beside the density correction, no other NDIR signal correction addressing a band broadening effect as a consequence of $CO_2$–$H_2O$ molecule interactions or any other $H_2O$ cross sensitivity is explicitly included in the sensor-sided data processing at this point. These aspects are considered through the in-water calibration, as mentioned in section 3.

Since the consideration of the zeroings requires an interpolation in time, this calculation step is best applied during postprocessing of field data to obtain a smooth behavior. To achieve the best measurement accuracy, changes in the sensor characteristics should also be included in the processing. Therefore, an interpolation between the polynomial of a predeployment calibration and the polynomial of a postdeployment calibration over the course of the deployment is conducted. We apply an interpolation that is not linear with time, but instead linear with the actual value of the zero signal throughout a deployment, $S_{2beam,Z}(t)$. The predeployment polynomial is transformed to the postdeployment polynomial by proportionately using the coefficients of the two polynomials according to the actual zero signal. This approach assumes a causal relationship between the temporally often nonlinear change in the zero signal and the change in concentration-dependent sensor response.

The entire calibration calculations and the postprocessing are accomplished with custom-designed LabVIEW routines (National Instruments, Austin, Texas).

## 5. Field evaluation

Field evaluations of the new $pCO_2$ sensor were carried out in April/May 2010 during a 6-week cruise in the North and South Atlantic (R/V *Polarstern*, ANT-XXVI/4) and in June–July 2011 during a 4-week cruise in the eastern tropical Atlantic (R/V *Maria S. Merian*, MSM-18/3; Fig. 5). During these cruises, oligotrophic (i.e., subtropical gyres) and mesotrophic regions (e.g., continental shelfs, equatorial upwelling) provided a reasonably wide range in $pCO_2$ (295–430 $\mu$atm; cf. Fig. 6 and Fig. 7, top panel) and temperature (7.4°–30.3°C, Fig. 5). Furthermore, strong $pCO_2$ and temperature gradients were found near hydrographic fronts. Thus, the conditions were ideal for a thorough evaluation of the sensor, which was tested during both cruises in nearly identical underway setups: Seawater, either supplied by the ship's clean seawater supply systems (ANT-XXVI/4) or by a submersible pump installed in the moon pool near the ship's keel (MSM-18/3), was pumped to the laboratory into a thermally insulated flow-through box (80-L volume) at a flow rate of approximately 12 L min$^{-1}$. Sea surface temperature (SST) and sea surface salinity (SSS) were determined for both cruises at the seawater intake. A sensor package containing the $pCO_2$ sensor (two units during ANT-XXVI/4, HC1 and HC2; one unit on MSM-18/3, HC3) and an oxygen optode (model 3830 or 4330, Aanderaa Data Instruments AS, Bergen, Norway), which also provided the water temperature in the flow-through box with an accuracy of ±0.05°C, were placed in the underway box. Data were binned into 1-min intervals. Since the $pCO_2$ sensor data were initially stored at 5-s intervals, the transformation to the 1-min intervals

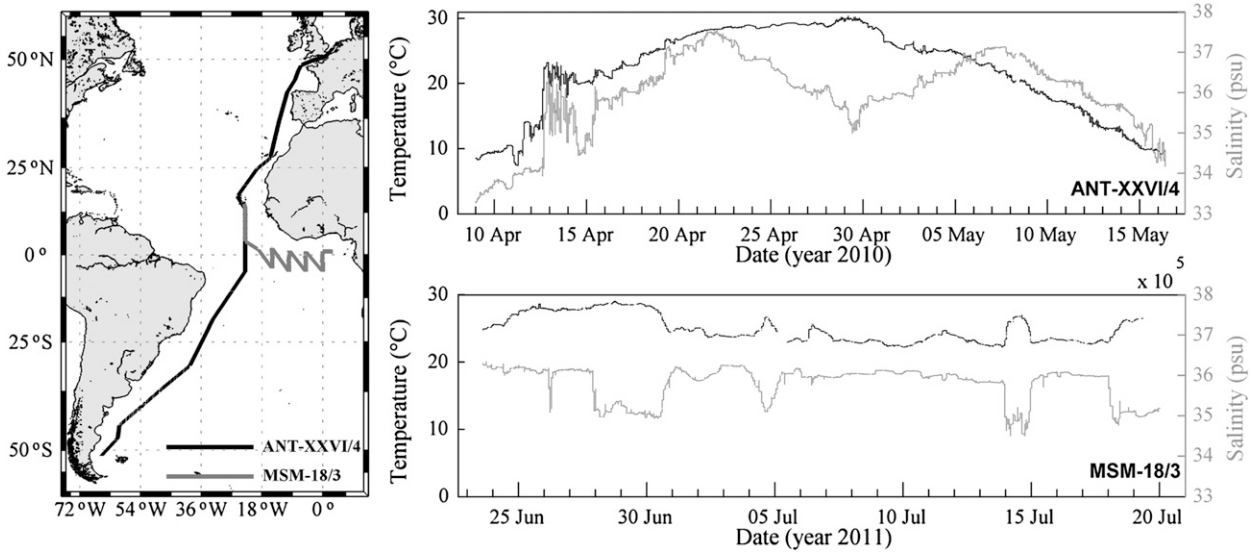


FIG. 5. (left) The cruise track of R/V *Polarstern* cruise ANT-XXVI/4 and R/V *Maria S. Merian* cruise MSM-18/3, and (right) the encountered SSS and temperature. R/V *Polarstern* sailed from Germany to Chile and R/V *Maria S. Merian* from Cape Verde to Gabon.

represents an averaging of typically 12 spot values. Zeroings were carried out every 12 h. The membrane interface of the $pCO_2$ sensor was supplied with a constant seawater flow by a SBE 5T pump (Sea-Bird Electronics Inc., Bellevue, Washington). A fully automated $pCO_2$ underway instrument (GO, General Oceanics, Miami, Florida; Pierrot et al. 2009) based on a spray head equilibrator and a LI-7000 $CO_2$ analyzer was operated in parallel. Throughout the expeditions and beside the deployment in the flow-through box, the sensors were additionally used for measurements on a CTD rosette system (HC1 and HC3; part of the data shown in Fiedler et al. 2013) and on a surface drifter (HC3; data not shown here; Steinhoff et al. 2011).

Sensors HC1 and HC2 were calibrated at 19.67°C before and after the deployment. HC3 was pre- and postcalibrated at 27.00° and 26.00°C, respectively.

The averaged sensor data were prepared for processing by filtering for obvious outlier zero values as, for example, caused by improper sensor warm-ups, as well as other outliers and data biased through insufficient water supply to the flow-through box. All $pCO_2$ sensor data recorded during flush and zero intervals were excluded from the comparison with the reference. The data of HC2 obtained between 28 April and 4 May were excluded from the comparison as well, as the excessively high water temperature did not allow for temperature stabilization at the calibration control temperature anymore. Although the control temperature within HC1 also temporarily exceeded the set point, no data were removed here, as the unit seemed to be more robust in this respect as compared to HC2.

Figures 6 and 7 show the $pCO_2$ measured by the flow-through reference system as well as the $pCO_2$ data of the HC1–3 sensors with all datasets corrected to SST for direct comparison (Takahashi et al. 1993). In addition, the $pCO_2$ differences ($\Delta pCO_2$) between the sensor and the reference ($pCO_{2,GO}$) are plotted versus time. The three $\Delta pCO_2$ curves for every sensor are related to different drift compensation mechanisms:

1) precalibration, no zeroings
2) precalibration + zeroings
3) precalibration + zeroings + postcalibration

In the case of (1) only the dual-beam correction is applied and the polynomial of the predeployment calibration is used for the entire dataset. Since in this case data are processed by referencing all signals to the zeroing carried out during shore-based calibration, large offsets can already occur at the beginning of a deployment because of a sensor drift that occurred during storage and transport or because of measurement conditions that strongly deviate from calibration conditions. Also, more or less strong drift behavior is observed over time. When the regular zero correction is carried out as described above (section 4), both initial offsets and drift over the course of the deployment are strongly reduced, demonstrating the effectiveness of this first correction. However, even smaller residuals were obtained when both zeroings and pre- and the postdeployment calibration polynomials are considered in the postprocessing (section 4). Table 2 shows the statistics of the $pCO_2$ residuals as obtained by this optimized processing

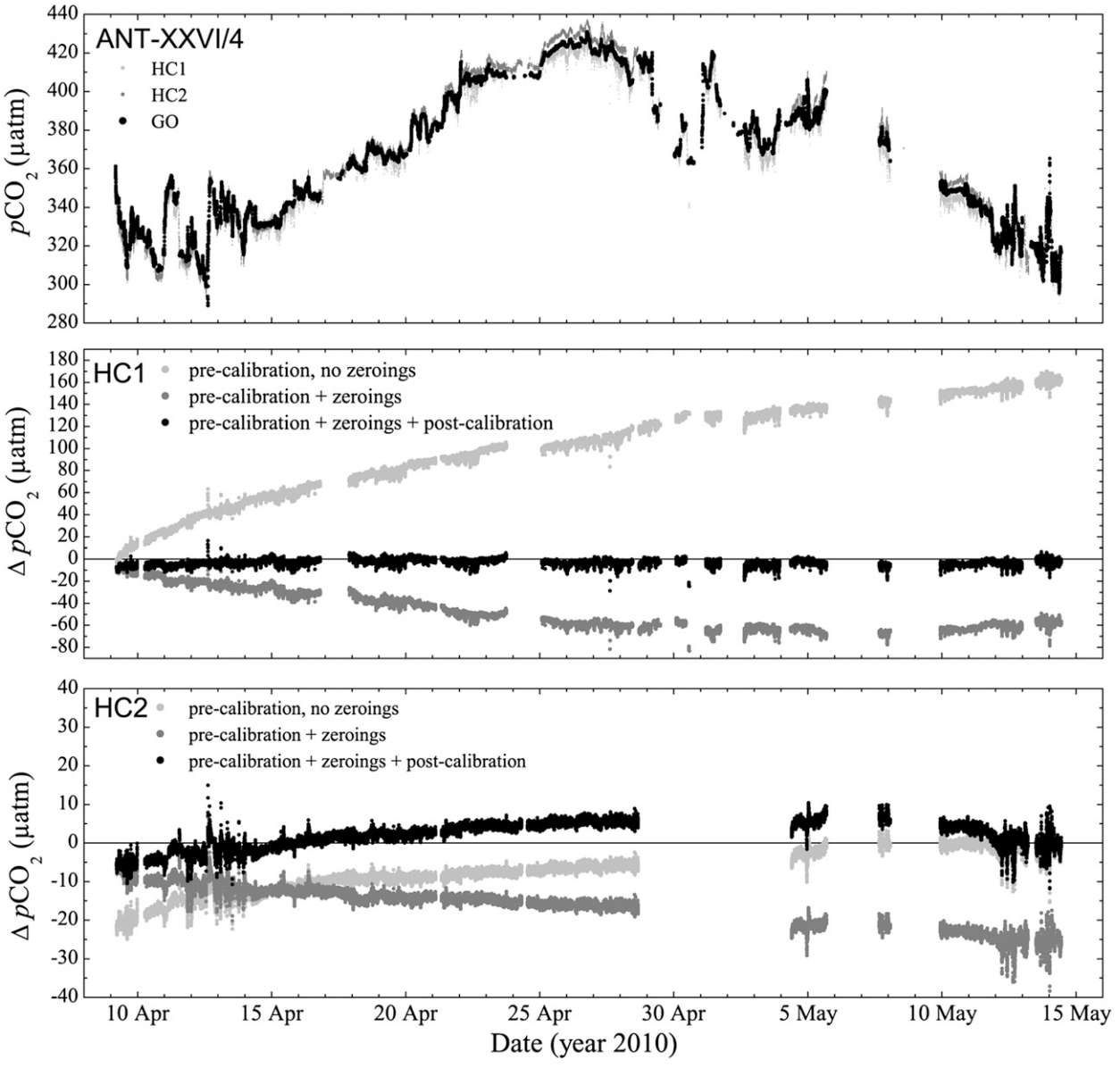


FIG. 6. The $pCO_2$ data obtained by (top) the GO system and HydroC sensors (middle) HC1 and (bottom) HC2 during ANT-XXVI/4. (top) The absolute values, and (middle),(bottom) the differences between the HydroC–$pCO_2$ and the reference ($\Delta pCO_2$) over time for three different processing methods in order to visualize the potential of different drift compensation mechanisms (refer to text). The black curve of HC1 and HC2 represents the final drift-corrected and postprocessed signal. Refer to the text for further details on the different processing methods as well as the peculiarities of strongly drifting HC1.

routine. In all three sensor deployments, the mean $pCO_2$ offset to the reference system is within $\pm 3\,\mu$atm. With an average $pCO_2$ residual over all three sensors of $-0.6$ $\pm 3.0\,\mu$atm (RMSE = $3.7\,\mu$atm), no systematic offset between $pCO_2$ sensor and reference system could be found. This indicates that the agreement between sensor and flow-through system $pCO_2$ is of similar magnitude as the accuracy of the flow-through system, which was estimated at $2\,\mu$atm (Pierrot et al. 2009). We use the mean RMSE from all three deployments of $3.7\,\mu$atm as a conservative estimate of the sensor accuracy. This result is very promising, as the sensors were only calibrated at a single water temperature and experienced a large temperature range during deployment (>20°C). We note that during these field tests, the sensors ran autonomously and without maintenance but were also used in other tests (e.g., deployments of CTD rosette casts; part of the data shown in Fiedler et al. 2013). For

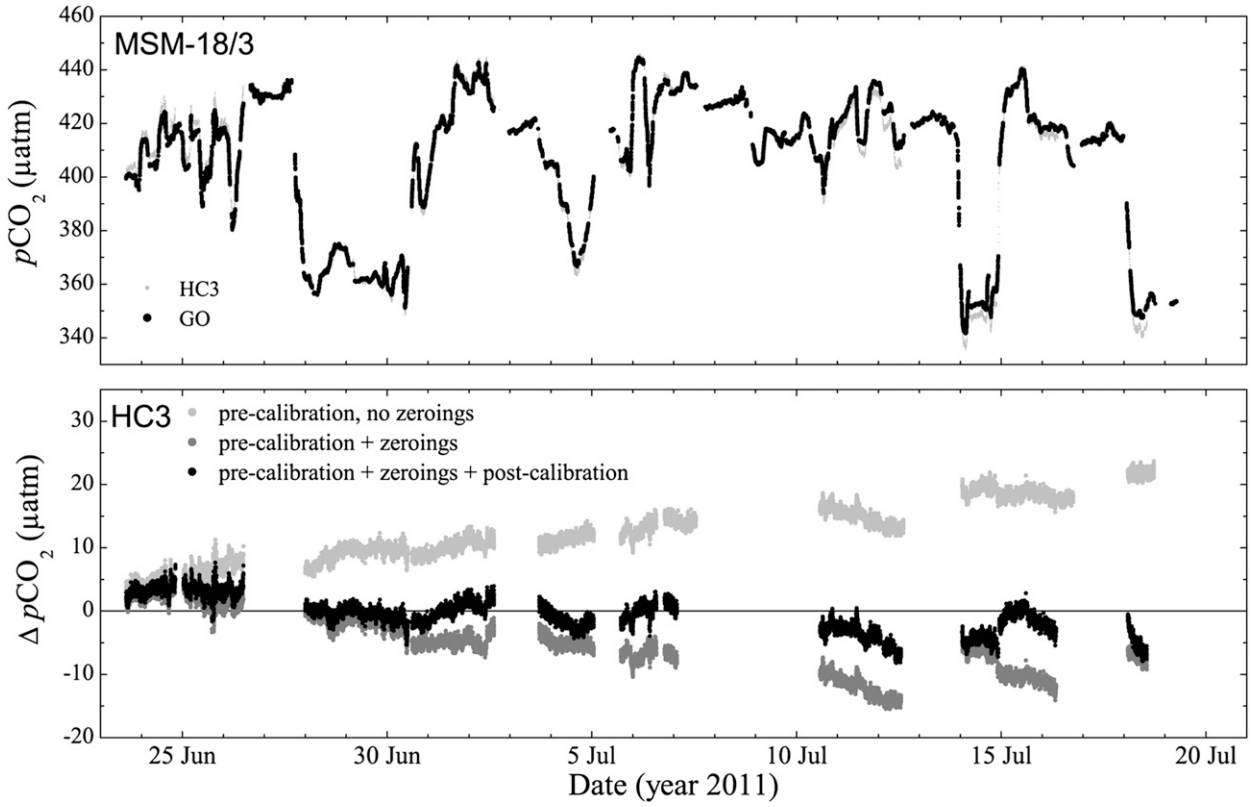


FIG. 7. (top) The $pCO_2$ trace during MSM-18/3 measured by the GO reference $pCO_2$ system and the HydroC sensor HC3. (bottom) The $pCO_2$ residuals between the HydroC and the reference ($\Delta pCO_2$) for three different drift compensation scenarios; the black curve represents the final drift-corrected and postprocessed signal.

this purpose the instruments had to be restarted several times. This appears to not have affected sensor performance negatively, since sensor HC3 was restarted most frequently but shows the smallest overall offset.

The compensation routines applied, which exclusively rely on data measured by the sensors themselves and the information obtained from calibrations, account well for the signal drift for all three sensors. After processing the data do not exhibit significant unaccounted drift behavior. This is even the case for the most strongly drifting sensor HC1, whose signal change over time is also reflected by the change in its calibration polynomials (Fig. 4). Although an NDIR detector drifting as strongly as in the case of HC1 would have failed current quality controls within the manufacturer's production, it is still a good example to demonstrate the effectiveness of the described processing algorithms. We would like to note that sensor HC1 also participated in a different sensor evaluation project (Tamburri et al. 2011). At that time, the sensor also showed a strong drift that could not be adequately compensated for because of a lack of full understanding of the required postprocessing steps that is presented here. Although the drift of HC1 could be well corrected for, in the end it still shows a slightly larger mean value and RMSE compared to HC2 and HC3. NDIR detectors that show a smaller zero drift typically show a smaller concentration-dependent signal change over time as well. This conclusion is further corroborated by the observation that a transformation of the predeployment into the postdeployment calibration polynomial based on the course of the zero values finally provides a better correction as opposed to a transformation assumed to occur linear in time (data not shown here).

To identify any remaining issues in the drift-corrected $pCO_2$ sensor data, the $\Delta pCO_2$ residuals were plotted against $pCO_{2,GO}$, SST, and $pH_2O$ (Fig. 8). All sensors show a weak correlation with all three parameters

TABLE 2. Statistics of the $\Delta pCO_2$ residuals for all three field deployments of the $pCO_2$ sensor with mean, standard deviation $\sigma$, and RMSE for a total of $n$ observations. Also shown is the mean of all three deployments.

| Sensor | Mean (µatm) | $\sigma$ (µatm) | RMSE (µatm) | $n$ |
|---|---|---|---|---|
| HC1 | −3.1 | 2.9 | 4.2 | 24 791 |
| HC2 | 1.8 | 3.4 | 3.9 | 24 163 |
| HC3 | −0.7 | 2.8 | 2.8 | 12 770 |
| Overall mean | −0.6 | 3.0 | 3.7 | |

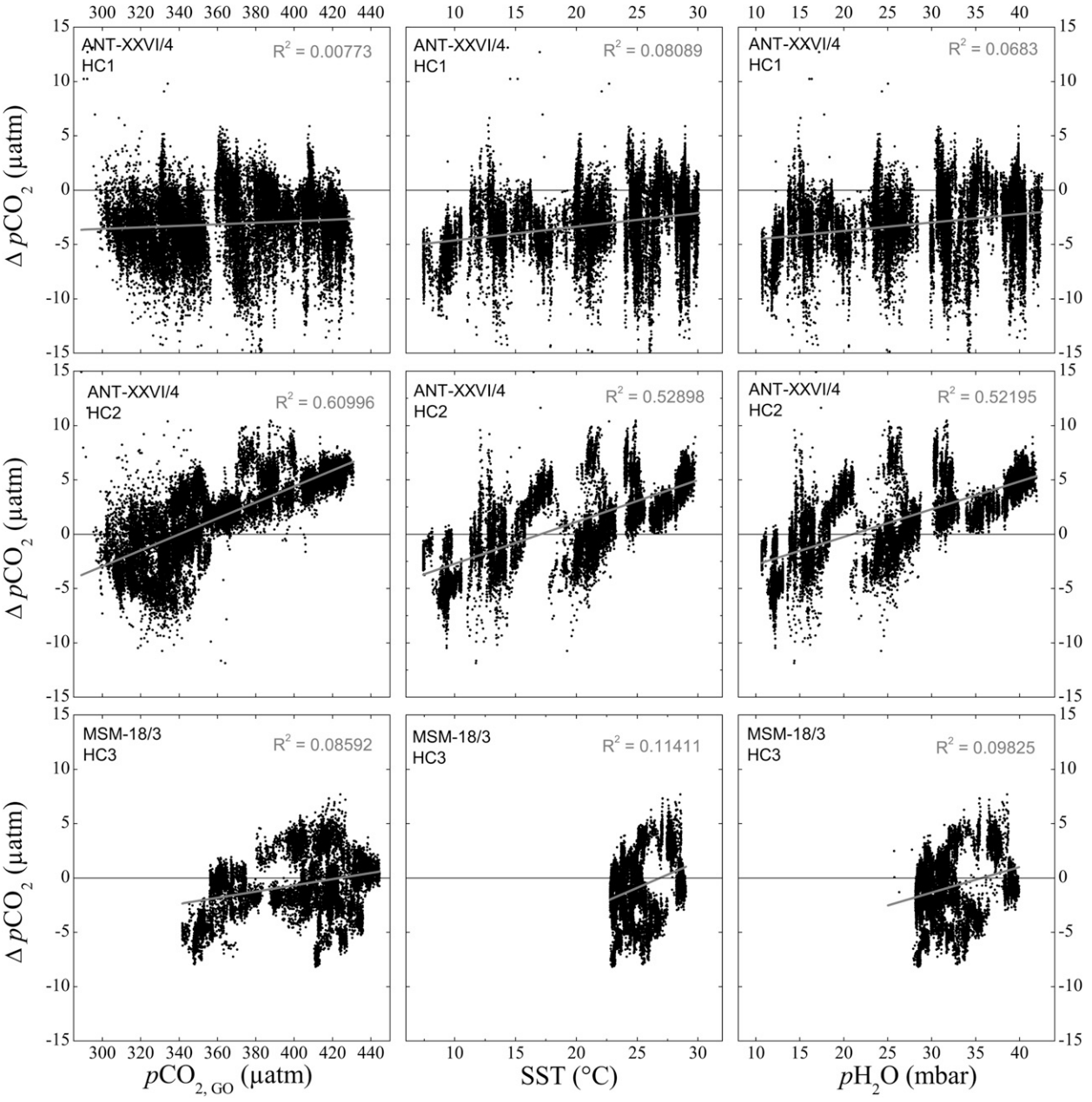


FIG. 8. (top) The residuals of HC1 vs (left) the reference $pCO_2$, (middle) the SST, and (right) the $pH_2O$ as measured within the internal gas stream close to the NDIR detector. (middle),(bottom) As in (top), but for HC2 and HC3, respectively. Although not statistically significant in all cases, a general positive correlation with all three parameters is discernible and is further discussed in the text.

($0.0 < R^2 < 0.6$), which is most clear for sensor HC2 ($0.5 < R^2 < 0.6$). Since $pCO_{2,GO}$, SST, and $pH_2O$ are strongly correlated in the field data, the cause of these remaining residual correlations cannot be clearly discerned. Nevertheless, there is indication for a weak NDIR signal dependency on $pH_2O$. In fact, $CO_2$ NDIR detectors overestimate in the presence of water vapor because of pressure broadening effects (McDermitt et al. 1993). Furthermore, the magnitude of this effect increases with $pCO_2$ and $pH_2O$. Since the sensor calibrations were only conducted at one temperature and band broadening effects due to varying water vapor concentrations are not considered within the sensor's data processing, this might explain at least part of the dependencies. The fact that HC2 and HC3 show the smallest $\Delta pCO_2$ around the water temperature at which they were calibrated support this observation. The limitations of the present dataset do not allow to further investigate this issue and additional tests

have to be carried out to assess the potential for further improvement, for example, by performing laboratory tests with and calibrations of the $pCO_2$ sensor at more than one temperature.

## 6. Summary and outlook

The development of a new underwater $pCO_2$ sensor based on membrane equilibration and NDIR spectrometry was described. Special emphasis was put on compensation measures for NDIR sensor drift as well as on the in-water calibration of the sensor. The performance of the $pCO_2$ sensor was assessed based on surface water field data obtained during two cruises, both lasting at least one month and covering a wide range in $pCO_2$ (289–445 $\mu$atm) and temperature (7.4°–30.1°C). A wet gas stream within a small underwater sensor represents a demanding environment for NDIR detectors. Against this background, the observed mean offset of $-0.6$ $\pm 3.0$ $\mu$atm with an RMSE of 3.7 $\mu$atm to the $pCO_2$ reference instrument as obtained through application of a pre- and postdeployment calibration in combination with regular zeroings is a very promising result, especially since the sensors were also used for various other measurements, including profiling applications in the water column during the deployments (data not part of this assessment). At a $pCO_2$ of 400 $\mu$atm, the observed mean $pCO_2$ difference corresponds to about 0.2% and the RMSE to less than 1%. This favorable result underlines the efficiency of the applied processing algorithms. The acquisition of high-quality field data by the new $pCO_2$ sensor calls for regular checks of the sensor parameters gas temperature, pressure, RH, and control temperature to guarantee optimal functioning of the sensor. In addition, regular zero gas measurements need to be carried out at least every 12 h under deployment conditions as a drift correction means beside the inherent single-beam dual wavelength setup of the sensor. To properly apply the zero information during postprocessing, measurement data should always be flanked by zeroings. In order to also account for the concentration-dependent effects on zero and dual-beam-corrected signals, the sensor needs to be recalibrated at different $pCO_2$ levels on a time scale of several months to a year to achieve the highest accuracies through data postprocessing. A water calibration as presented in this paper at a temperature close to the expected water temperatures in the field is beneficial. Nevertheless, the RMSE found within this work is based on field data obtained under conditions where water temperatures deviated by ±10°C from the calibration temperature.

The assessment given here represents an important milestone for the development of the sensor. The procedures discussed are planned to be further automated and implemented into data processing routines. The next development steps include investigation of potential improvements with respect to NDIR data processing and the laboratory calibration routines to identify and compensate for minor signal dependencies on water vapor and on changes in gas matrix composition as caused by, for example, strongly varying oxygen concentrations. Moreover, the long-term stability during deployments on moorings and profiling buoys in the water column will be investigated as well as the sensor performance on different moving platforms analyzed; especially the latter has been simplified by a recently released smaller and faster version of the HydroC.

*Acknowledgments.* The authors thank all members of the "$(C)O_2$" working group at the GEOMAR as well as Gernot Friedrichs from the CAU for the fruitful discussions and helpful advice. Furthermore, we thank the CONTROS team for its support in this development project. We explicitly acknowledge Christian Rettich for his assistance, especially during the construction of the first prototypes, as well as Claus Hinz and Matthias Lunge for their valuable help with laboratory experiments. Janna Bohlen and Christoph Kirbach are thanked for commenting on the manuscript. We would also like to thank the captains and crews of R/V *Polarstern* and *Maria S. Merian* for their assistance. This work was partly funded by the SAW project OCEANET of the Leibniz Association (2008–2010) and by the SOPRAN project of the German Federal Ministry of Education and Research (Grants 03F0462A and 03F0611A).

## REFERENCES

Byrne, R. H., and W. Yao, 2008: Procedures for measurement of carbonate ion concentrations in seawater by direct spectrophotometric observations of Pb(II) complexation. *Mar. Chem.,* **112,** 128–135, doi:10.1016/j.marchem.2008.07.009.

——, X. Liu, E. A. Kaltenbacher, and K. Sell, 2002: Spectrophotometric measurement of total inorganic carbon in aqueous solutions using a liquid core waveguide. *Anal. Chim. Acta,* **451,** 221–229, doi:10.1016/S0003-2670(01)01423-4.

——, and Coauthors, 2010: Sensors and systems for in situ observations of marine carbon dioxide system variables. *Proceedings of OceanObs'09: Sustained Ocean Observations and Information for Society,* J. Hall, D. E. Harrison, and D. Stammer, Eds., ESA Publ. WPP-306, doi:10.5270/OceanObs09.cwp.13.

DeGrandpre, M. D., T. R. Hammar, S. P. Smith, and F. L. Sayles, 1995: In-situ measurements of seawater $pCO_2$. *Limnol. Oceanogr.,* **40,** 969–975.

Dickson, A. G., C. L. Sabine, and J. R. Christian, Eds., 2007: Guide to best practices for ocean $CO_2$ measurements. PICES Special Publ. 3, 191 pp.

Doney, S. C., V. J. Fabry, R. A. Feely, and J. A. Kleypas, 2009: Ocean acidification: The other $CO_2$ problem. *Annu. Rev. Mar. Sci.,* **1,** 169–192, doi:10.1146/annurev.marine.010908.163834.

Fiedler, B., P. Fietzek, N. Vieira, P. Silva, H. C. Bittig, and A. Körtzinger, 2013: In situ $CO_2$ and $O_2$ measurements on a profiling float. *J. Atmos. Oceanic Technol.,* **30,** 112–126.

Fietzek, P., S. Kramer, and D. Esser, 2011: Deployment of the HydroC ($CO_2$/$CH_2$) on stationary and mobile platforms—Merging the trends in the field of platform and sensor development. *Proc. Oceans '11 MTS/IEEE Kona,* Kona, Hawaii, MTS, IEEE/OES, Paper 110422-140. [Available online at http://ieeexplore.ieee.org/xpl/mostRecentIssue.jsp?punumber=6093765.]

Friedrichs, G., J. Bock, F. Temps, P. Fietzek, A. Körtzinger, and D. W. R. Wallace, 2010: Toward continuous monitoring of seawater $^{13}CO_2/^{12}CO_2$ isotope ratio and $pCO_2$: Performance of cavity ringdown spectroscopy and gas matrix effects. *Limnol. Oceanogr. Methods,* **8,** 539–551, doi:10.4319/lom.2010.8.539.

Gruber, N., and Coauthors, 2010: Towards an integrated observing system for ocean carbon and biogeochemistry at a time of change. *Proceedings of OceanObs'09: Sustained Ocean Observations and Information for Society,* J. Hall, D. E. Harrison, and D. Stammer, Eds., ESA Publ. WPP-306, doi:10.5270/OceanObs09.pp.18.

Johnson, K. S., and Coauthors, 2009: Observing biogeochemical cycles at global scales with profiling floats and gliders: Prospects for a global array. *Oceanography,* **22,** 216–224.

Körtzinger, A., H. Thomas, B. Schneider, N. Gronau, L. Mintrop, and J. C. Duinker, 1996: At-sea intercomparison of two newly designed underway $pCO_2$ systems—Encouraging results. *Mar. Chem.,* **52,** 133–145.

——, and Coauthors, 2000: The international at-sea intercomparison of $fCO_2$ systems during the RV Meteor cruise 36/1 in the North Atlantic Ocean. *Mar. Chem.,* **72,** 171–192, doi:10.1016/S0304-4203(00)00080-3.

Lefèvre, N., J. P. Ciabrini, G. Michard, B. Brient, M. DuChaffaut, and L. Merlivat, 1993: A new optical sensor for $pCO_2$ measurements in seawater. *Mar. Chem.,* **42,** 189–198, doi:10.1016/0304-4203(93)90011-C.

Martz, T. R., J. G. Connery, and K. S. Johnson, 2010: Testing the Honeywell Durafet for seawater pH applications. *Limnol. Oceanogr. Methods,* **8,** 172–184, doi:10.4319/lom.2010.8.172.

McDermitt, D. K., J. M. Welles, and R. D. Eckles, 1993: Effects of temperature, pressure and water vapor on gas phase infrared absorption by $CO_2$. LI-COR, Inc., 5 pp.

McNeil, C., E. D'Asaro, B. Johnson, and M. Horn, 2006: A gas tension device with response times of minutes. *J. Atmos. Oceanic Technol.,* **23,** 1539–1558.

Merkel, T. C., V. I. Bondar, K. Nagai, B. D. Freeman, and I. Pinnau, 2000: Gas sorption, diffusion, and permeation in poly (dimethylsiloxane). *J. Polym. Sci.,* **38B,** 415–434, doi:10.1002/(SICI)1099-0488(20000201)38:3<415::AID-POLB8>3.0.CO;2-Z.

Metz, B., O. Davidson, H. de Coninck, M. Loos, and L. Meyer, Eds., 2005: *Carbon Dioxide Capture and Storage.* Cambridge University Press, 431 pp.

Millero, F. J., 2007: The marine inorganic carbon cycle. *Chem. Rev.,* **107,** 308–341, doi:10.1021/cr0503557.

Pfeil, B., and Coauthors, 2013: A uniform, quality controlled Surface Ocean $CO_2$ Atlas (SOCAT). *Earth Syst. Sci. Data,* 125–143, doi:10.5194/essd-5-125-2013.

Pierrot, D., and Coauthors, 2009: Recommendations for autonomous underway $pCO_2$ measuring systems and data-reduction routines. *Deep-Sea Res. II,* **56,** 512–522, doi:10.1016/j.dsr2.2008.12.005.

Robb, W. L., 1968: Thin silicone membranes—Their permeation properties and some applications. *Ann. N. Y. Acad. Sci.,* **146,** 119–137.

Roemmich, D., G. C. Johnson, S. Riser, R. Davis, and J. Gilson, 2009: The Argo program: Observing the global ocean with profiling floats. *Oceanography,* **22,** 34–43.

Rogner, H.-H., D. Zhou, R. Bradley, P. Crabbé, O. Edenhofer, B. Hare, L. Kuijpers, and M. Yamaguchi, 2007: Introduction. *Climate Change 2007: Mitigation of Climate Change,* B. Metz et al., Eds., Cambridge University Press, 97–116.

Sabine, C. L., and Coauthors, 2004: The oceanic sink for anthropogenic $CO_2$. *Science,* **305,** 367–371.

Saderne, V., P. Fietzek, and P. M. J. Herman, 2013: Extreme variations of $pCO_2$ and pH in a macrophyte meadow of the Baltic Sea in summer: Evidence of the effect of photosynthesis and local upwelling. *PLoS One,* **8,** e62689, doi:10.1371/journal.pone.0062689.

Seidel, M. P., M. D. DeGrandpre, and A. G. Dickson, 2008: A sensor for in situ indicator-based measurements of seawater pH. *Mar. Chem.,* **109,** 18–28, doi:10.1016/j.marchem.2007.11.013.

Severinghaus, J. W., and A. F. Bradley, 1958: Electrodes for blood $pO_2$ and $pCO_2$ determination. *J. Appl. Physiol.,* **13,** 515–520.

Stow, R. W., R. F. Baer, and B. F. Randall, 1957: Rapid measurement of the tension of carbon dioxide in blood. *Arch. Phys. Med. Rehabil.,* **38,** 646–650.

Takahashi, T., 1961: Carbon dioxide in the atmosphere and in Atlantic Ocean water. *J. Geophys. Res.,* **66,** 477–494.

——, J. Olafsson, J. G. Goddard, D. W. Chipman, and S. C. Sutherland, 1993: Seasonal variation of $CO_2$ and nutrients in the high-latitude surface oceans: A comparative study. *Global Biogeochem. Cycles,* **7,** 843–878.

——, and Coauthors, 2009: Climatological mean and decadal change in surface ocean $pCO_2$, and net sea–air $CO_2$ flux over the global oceans. *Deep-Sea Res. II,* **56,** 554–577, doi:10.1016/j.dsr2.2008.12.009.

Tamburri, M. N., and Coauthors, 2011: Alliance for coastal technologies: Advancing moored $pCO_2$ instruments in coastal waters. *Mar. Technol. Soc. J.,* **45,** 43–51, doi:10.4031/MTSJ.45.1.4.

Wang, Z. A., X. Liu, R. H. Byrne, R. Wanninkhof, R. E. Bernstein, E. A. Kaltenbacher, and J. Patten, 2007: Simultaneous spectrophotometric flow-through measurements of pH, carbon dioxide fugacity, and total inorganic carbon in seawater. *Anal. Chim. Acta,* **596,** 23–36.

Watson, A. J., and Coauthors, 2009: Tracking the variable North Atlantic sink for atmospheric $CO_2$. *Science,* **326,** 1391–1393, doi:10.1126/science.1177394.

Weiss, R. F., 1974: Carbon dioxide in water and seawater: The solubility of a non-ideal gas. *Mar. Chem.,* **2,** 203–215.

Wiegleb, G., and Coauthors, 2001: *Industrielle Gasssensorik: Messverfahren—Signalverarbeitung—Anwendungstechnik—Prüfkriterien.* Expert-Verlag, 164 pp.